Bioorganic & Medicinal Chemistry Letters 19 (2009) 5321–5324

Contents lists available at ScienceDirect

Bioorganic & Medicinal Chemistry Letters

journal homepage: www.elsevier.com/locate/bmcl

Improving potency and selectivity of a new class of non-Zn-chelating MMP-13 inhibitors

Alexander Heim-Riether [a,*], Steven J. Taylor [a], Shuang Liang [a], Donghong Amy Gao [a], Zhaoming Xiong [a], E. Michael August [a], Brandon K. Collins [a], Bennett T. Farmer II [a], Kathleen Haverty [a], Melissa Hill-Drzewi [a], Hans-Dieter Junker [c], S. Mariana Margarit [a], Neil Moss [a], Thomas Neumann [c], John R. Proudfoot [a], Lana Smith Keenan [a], Renate Sekul [c], Qiang Zhang [a], Jun Li [b], Neil A. Farrow [a]

[a] Boehringer Ingelheim Pharmaceuticals, Department of Medicinal Chemistry, 900 Ridgebury Rd, Ridgefield, CT 06877, USA
[b] Boehringer Ingelheim Pharmaceuticals, Department of Immunology and Inflammation, 900 Ridgebury Rd, Ridgefield, CT 06877, USA
[c] Graffinity Pharmaceuticals GmbH, Im Neuenheimer Feld 518, 69120 Heidelberg, Germany

ARTICLE INFO

Article history:
Received 3 July 2009
Revised 27 July 2009
Accepted 29 July 2009
Available online 3 August 2009

Keywords:
MMP-13
Non-Zn-chelating inhibitor
SAR

ABSTRACT

Discovery and optimization of potency and selectivity of a non-Zn-chelating MMP-13 inhibitor with the aid of protein co-crystal structural information is reported. This inhibitor was observed to have a binding mode distinct from previously published MMP-13 inhibitors. Potency and selectivity were improved by extending the hit structure out from the active site into the S1′ pocket.

Matrix metalloproteinases (MMPs) are zinc- and calcium dependent endopeptidases involved in the degradation of extracellular matrix and tissue remodeling.[1] MMP-13, the most efficient type II collagen-degrading MMP,[2] is an attractive therapeutic target because evidence supports it playing a critical role in the pathogenesis of osteoarthritis (OA).[3] Broad-spectrum MMP inhibitors have failed in clinical trials at least in part due to a painful, joint-stiffening side effect, termed musculoskeletal syndrome (MSS).[4] It is believed that MSS is caused by the inhibition of normal extracellular matrix turnover, likely due to the inhibition of MMPs other than MMP-13.[5] The extent to which other MMPs contribute to MSS is not well understood. Nevertheless, we sought to develop MMP-13 inhibitors with high isoform selectivity to mitigate unperceived risk associated with inhibiting other isoforms.

MMPs have a conserved active site motif, where a tris(histidine)-bound zinc(II) acts as the catalytic site for substrate hydrolysis. Historically, most MMP inhibitors gained affinity through interacting with the catalytic zinc via a chelating moiety (e.g., hydroxamic acid) and by positioning hydrophobic functionality in the S1′ pocket.[4a,6] The S1′ pocket is in part formed by the selectivity loop which varies in length and amino acid sequence for different MMP isoforms. These S1′ differences between MMP family members have been utilized to design MMP inhibitors with different selectivity profiles.[7] MMP-13 has an additional region for inhibitor binding that has not been observed in other MMP isoforms. This region is referred to as the S1′* pocket. At present, the most potent and selective MMP-13 inhibitors occupy both the S1′ and S1′* pockets.[8] The potency provided by binding to the S1′ and S1′* sites reduces the need for inhibitors to require a Zn binding group.

Through a Graffinity SPR microarray screening campaign,[9] we identified hit structure **1** that was subsequently determined to have an IC_{50} of 430 nM against MMP-13 (Scheme 1). Compound **1** attracted our attention since it did not contain an obvious Zn-chelating group and showed selectivity over MMP-14 (Table 1)—the one isoform postulated to play a role in MSS.[5] We obtained a co-structure of **1** with MMP-13 which revealed a binding mode not previously observed for a compound lacking a Zn-chelating group (Fig. 1).

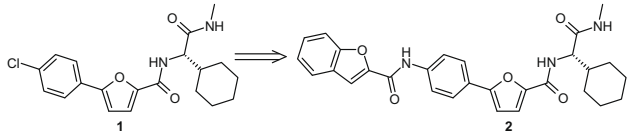

Scheme 1. Screening hit and first modification.

* Corresponding author. Tel.: +1 203 798 5579; fax: +1 203 791 6072.
E-mail address: alexander.heim-riether@boehringer-ingelheim.com (A. Heim-Riether).

0960-894X/$ - see front matter © 2009 Elsevier Ltd. All rights reserved.
doi:10.1016/j.bmcl.2009.07.151

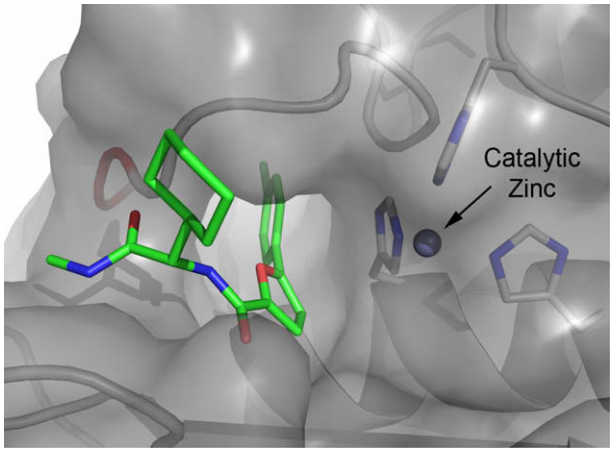

Figure 1. MMP13-co-crystal structure of compound **1**. No interaction to the catalytic Zn is observed; entrance of S1′ pocket is occupied by phenyl ring.[10]

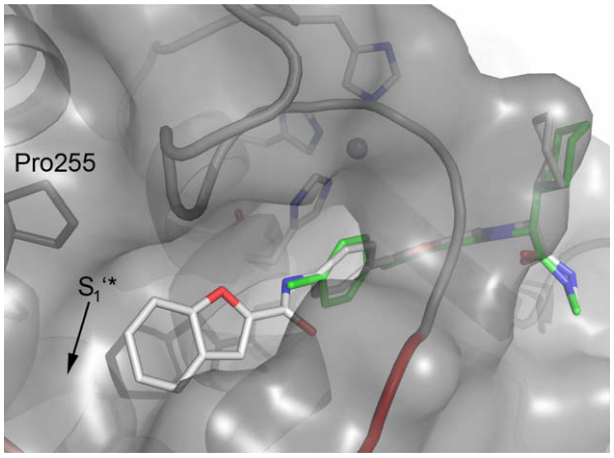

Figure 2. Overlay of co-crystal structures of compound **1** (green) and **2** (gray) within the S1′ pocket of MMP-13. **2** reaches deeper into the S1′ pocket (selectivity loop highlighted in red).[10]

Compound **1** binds in the active site region despite not interacting with the catalytic zinc. The observed key interactions are three hydrogen bonds from and to the amino acid portion of the molecule and a π-stacking interaction of the phenyl ring with one of the histidines.[10] Since it is not precedented that potency and selectivity can be easily gained through interactions in the active site, we focused our attention on the observation that compound **1** does not fill the S1′ pocket. The phenyl ring occupies only the entrance to the S1′ pocket thus providing the opportunity to grow into the S1′ pocket to improve potency against MMP-13 and the overall selectivity profile against additional MMP isoforms. This opportunity and the distinctly different binding mode compared to other known MMP-13 inhibitors made **1** an attractive starting point for a discovery program.

Our initial attempt at expanding compound **1** to fill the unoccupied S1′ pocket involved replacing the chlorine with a benzofuran carboxamide (compound **2**, Scheme 1). This modification was based on published SAR of a Zn-chelating, partially selective MMP-13 inhibitor.[6] Compound **2** was essentially equipotent to compound **1** but provided an improved selectivity profile against a panel of MMP isoforms (Table 1).

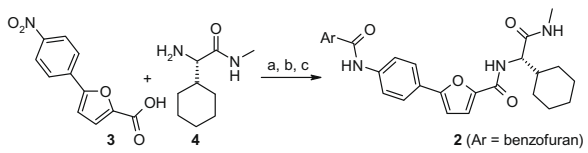

Scheme 2. Reagents: (a) EDC, HOBt, DIEA, DCM; (b) Zn, AcOH; (c) $ArCO_2H$, HATU, DIEA, DMF.

A co-structure of **2** with MMP-13 showed the benzofuran moiety occupying the S1′ pocket (Fig. 2, compound **2** in gray). No specific interactions of the benzofuran carboxamide with the protein were observed,[10] which may explain the lack of potency increase. The selectivity gain against other isoforms was attributed to differences in shape and size of the S1′ pockets which are defined in part by the amino acid sequences and lengths of the respective selectivity loops of the various isoforms. Compared to MMP-13, this loop is one to two amino acids shorter for some isoforms (MMP-1, -2, -9, -11), presumably leading to a smaller S1′ pocket that does not

Table 1
Aniline amide SAR[11]

Compd	Ar	MMP-13 IC_{50} (nM)	MMP-1	MMP-2	MMP-3	MMP-7	MMP-8	MMP-9	MMP-10	MMP-12	MMP-14
			Fold over MMP-13								
1	—	430	>50	6	28	>50	2	9	9	5	>100
2		620	>30	>100	>30	>30	>30	>30	4	>30	>100
5		63	>100	>100	13	>100	>100	>100	4	>100	>100
6		57	>100	73	3	>100	>100	>100	1	51	>100
7		31	>100	63	3	>100	>100	>100	1	33	>100
8		180	>100	30	8	>100	>100	>100	4	26	>100
9		88	>100	>100	7	>100	>100	>100	2	>100	>100
10		17	>1000	>1000	37	>1000	>1000	>1000	21	>1000	>1000

accommodate the benzofuran. For MMP-3 and -10 the loop is one amino acid longer, presumably leading to a larger S1′ pocket. This may in part explain the low selectivity of compound **2** against MMP-10.

Although the gain in selectivity for compound **2** over **1** was encouraging, affinity for MMP-13 and selectivity against MMP-10 needed improvement. Based on the co-crystal structure of **2** it was apparent that extensions from the 4- and 5-position of the benzofuran had the potential to improve potency and selectivity by leveraging the S1′* pocket. However, such modifications would result in significant increases in molecular weight (**2**: MW = 499).

We focused on identifying groups that took better advantage of the potentially unique shape of the S1′ pocket of MMP-13 compared to other isoforms. A lipophilic residue proximal to the specificity loop, proline 255, further distinguishes MMP-13 from most MMPs in our panel which have a polar residue at this position (MMP-2, -3, -7, -9, -10, -12: serine). It turned out that groups smaller than the benzofuran provided interesting potency and selectivity profiles (Table 1). These compounds were prepared in a straight forward manner as shown in Scheme 2.

Compound **5** led to a 10-fold increase in potency against MMP-13 but this was accompanied by a decrease in selectivity against MMP-3. MMP-3 is the other MMP in the panel possessing a selectivity loop one amino acid longer than MMP-13. Therefore, further reducing the size of the group occupying the S1′ pocket might be expected to cause an additional loss in selectivity against MMP-3 and -10. This was supported by removing one of the methyl groups of **5** to provide compound **6** which, while equipotent against MMP-13, lost selectivity against MMP-2, -3, -10 and -12. Similar trends in potency and selectivity were observed when switching from the furanyl to the pyrazole ring system (compounds **7**–**9**). However, the most significant advance came from incorporating a methyl pyridyl group, leading to compound **10** which combines improved potency with an overall improved selectivity profile compared to compound **2**.

While compound **10** demonstrated a more attractive balance of potency and selectivity than **2**, the terminal aryl amide linkage was considered a liability since hydrolysis would lead to a potentially mutagenic fragment. Alternative linkages without the terminal aryl group were surveyed (Table 2). A straightforward synthesis is shown in Scheme 3.

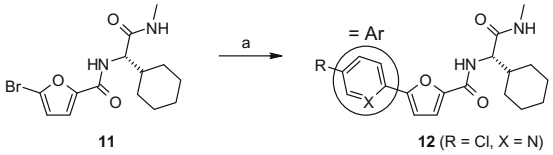

11 12 (R = Cl, X = N)

Scheme 3. Reagents and conditions: (a) 4-R-ArB(OH)$_2$ (Ar = Ph, pyridyl), Pd(PPh$_3$)$_4$, 2 M Na_2CO_3, DMF, 80–120 °C.

Table 2
Baseline compounds (**13**–**20**) for alternative functionalities to connect the terminal aryl group to the core

Compds	R	X	MMP-13 IC_{50} (nM)	HT-Sol pH 4.5/7.4 (μg/mL)
1	Cl	CH	430	1.5/1.9
12	Cl	N	245	35/37
13	MeC(=O)NH–	CH	1550	15/17
14	MeNHC(=O)–	CH	6000	16/17
15	$MeSO_2NH$–	CH	460	53/61
16	$MeNHSO_2$–	CH	480	50/52
17	H_3C–	CH	290	—
18	PhO–	CH	>50,000	—
19	MeO–	CH	220	1.4/1.6
20	EtO–	N	32	33/>49

Interestingly, acetamide **13**, the de-arylated analogue of the terminal aryl SAR of Table 1, was together with its reversed amide isomer **14** among the least potent analogs tested. Based on its potency, small size, chemical feasibility and the potential to mimic the 2-atom-linkage of the amide, the ether linkage contained in **19** and **20** was selected for subsequent terminal aryl SAR (Table 3). Analogue **20**, derived from the combination of the ether linkage of **19** with the pyridyl ring of compound **12**, promised not only the potential for more potent but also relatively soluble inhibitors. Combinations with the aryl ether functionality are highlighted in Table 3 and they were synthesized using the synthetic sequence as illustrated in Scheme 4.

Adding our most selective aryl groups, the benzofuran of compound **2** and the methylpyridine of **10**, to the ether linkage revealed different trends for potency and selectivity compared to

Table 3
Benzylether SAR (compounds are selective against MMP-1, -7, and -14)[11]

Compds	R	MMP-13 IC_{50} (nM)	MMP-2	MMP-3	MMP-8	MMP-9	MMP-10	MMP-12	HT-Sol pH 4.5/7.4 (μg/mL)
			Fold over MMP-13						
20	H_3C	32	4	8	5	1	5	10	33/>49
24	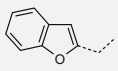	6	>500	26	>500	>500	11	>1000	<0.1/0.1
25		40	21	4	>500	>100	6	68	7.4/3.4
26		6	6	21	>100	4	14	>100	39/43
27	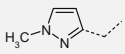	25	10	7	>100	>100	6	21	—
28	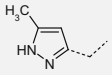	2	19	80	>1000	65	64	>500	25/31
29	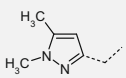	4	>100	45	>500	>500	24	>100	>57/>57

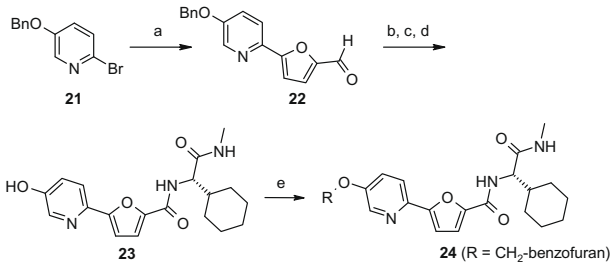

Scheme 4. Reagents and conditions: (a) 2-furaldehyde-4-boronic acid, $Pd(PPh_3)_4$, 2 M Na_2CO_3, DME, 120 °C; (b) $NaClO_2$, NaH_2PO_4, $HOSO_2NH_2$, dioxane; (c) (*S*)-2-amino-2-C_6H_{11}-*N*-methyl-acetamide, TBTU, DIEA, DMF; (d) 10% Pd/C, 1,4-cyclohexadiene, EtOAc, MeOH; (e) $ArCH_2OH$, DIAD, PPh_3, THF.

the corresponding amide analogs. Compound **24**, the combination of the benzofuran with the ether linkage, was significantly more potent than its amide counterpart **2** while maintaining a similar selectivity profile. In contrast, the methylpyridine ether analogue **25** demonstrated comparable potency to the corresponding amide linked compound **10**, but surprisingly, lost selectivity against MMP-2, -3, -10, and -12. However, it turned out that the more soluble pyrazole ether combinations (**26**–**29**) depending on the substitution pattern can best balance both potency and selectivity. Dimethylpyrazole **29**, the combination of N-and C-methylated pyrazoles **27** and **28**, respectively, became the most potent and selective MMP-13 inhibitor of the series.

In summary, we have reported the optimization of a novel class of non-Zn-chelating MMP-13 inhibitors with the aid of co-crystal structural information. The hit structure was extended out from the active site into the S1′ pocket by adding an aryl group through two different linking functionalities. Depending on the linkage different trends for potency and selectivity for the respective aryl groups were observed. Compounds with excellent potency and acceptable selectivity profiles were obtained.

References and notes

1. (a)*Matrix Metalloproteinases and TIMPs*; Woessner, J. F., Nagase, H., Eds.; Oxford University Press: New York, 2000; (b) Cawston, T. E.; Wilson, A. J. *Best Pract. Res., Clin. Rheumatol.* **2006**, *20*, 983; (c) Huxley-Jones, J.; Foord, S. M.; Barnes, M. R. *Drug Discovery Today* **2008**, *13*, 685.
2. Knäuper, V.; Will, H.; Lopez-Otin, C.; Smith, B.; Atkinson, S. J.; Stanton, H.; Hembry, R. M.; Murphy, G. *J. Biol. Chem.* **1996**, *271*, 17124.
3. Recent review: (a) Rowan, A. D.; Litherland, G. J.; Hui, W.; Milner, J. M. *Exp. Opin. Ther. Targets* **2008**, *12*, 1. and references therein; (b) Mitchell, P. G.; Magna, H. A.; Reeves, L. M.; Lopresti-Morrow, L. L.; Yocum, S. A.; Rosner, P. J.; Geoghegan, K. F.; Hambor, J. E. *J. Clin. Invest.* **1996**, *97*, 761; (c) Reboul, P.; Pelletier, J.-P.; Tardif, G.; Cloutier, J.-M.; Martel-Pelletier, J. *J. Clin. Invest.* **1996**, *97*, 2011; (d) Wernicke, D.; Seyfert, C.; Hinzmann, B.; Gromnica-Ihle, E. *J. Rheumatol.* **1996**, *23*, 590; (e) Billinghurst, R. C.; Dahlberg, L.; Ionescu, M.; Reiner, A.; Bourne, R.; Rorabeck, C.; Mitchell, P.; Hambor, J.; Diekmann, O.; Tschesche, H.; Chen, J.; Van Wart, H.; Poole, A. R. *J. Clin. Invest.* **1997**, *99*, 1534; (f) Freemont, A. J.; Byers, R. J.; Taiwo, Y. O.; Hoyland, J. A. *Ann. Rheum. Dis.* **1999**, *58*, 357.
4. (a) Skiles, J. W.; Gonnella, N. C.; Jeng, A. Y. *Curr. Med. Chem.* **2001**, *8*, 425; (b) Clark, I. M.; Parker, A. E. *Exp. Opin. Ther. Targets* **2003**, *7*, 19; (c) Renkiewicz, R.; Qiu, L.; Lesch, C.; Sun, X.; Devalaraja, R.; Cody, T.; Kaldjian, E.; Welgus, H.; Baragi, V. *Arthritis Rheum.* **2003**, *48*, 1742.
5. Historically, MMP-1 and -14 were the postulated key players in causing MSS. However, the non-selective MMP-13 inhibitor CP-544439, which is inactive against MMP-1, has caused MSS in clinical trials: Reiter, L. A.; Freeman-Cook, K. D.; Jones, C. S.; Martinelli, G. J.; Antipas, A. S.; Berliner, M. A.; Datta, K.; Downs, J.; Eskra, J. D.; Forman, M. D.; Greer, E. M.; Guzman, R.; Hardink, J. R.; Janat, F.; Keene, N. F.; Laird, E. R.; Liras, J.; Lopresti-Morrow, L. L.; Mitchell, P. G.; Pandit, J.; Robertson, D.; Sperger, D.; Vaughn-Bowser, M. L.; Waller, D. M.; Yocum, S. A. *Bioorg. Med. Chem. Lett.* **2006**, *16*, 5822. MMP-14 has KO mice data supporting it being a strong candidate for MSS: see Ref. 3a.
6. (a) Wu, J.; Rush, T. S.; Hotchandani, R.; Du, X.; Geck, M.; Collins, E.; Xu, Z.-B.; Skotnicki, J.; Levin, J. I.; Lovering, F. E. *Biorg. Med. Chem. Lett.* **2005**, *15*, 4105; (b) Li, J.; Rush, T. S.; Li, W.; DeVincentis, D.; Du, X.; Hu, Y.; Thomason, J. R.; Xiang, J. S.; Skotnicki, J. S.; Tam, S.; Cunningham, K. M.; Chockalingam, P. S.; Morris, E. A.; Levin, J. I.; Lovering, F. E. *Biorg. Med. Chem. Lett.* **2005**, *15*, 4961.
7. Matter, H.; Schudok, M. *Curr. Opin. Drug Discovery Dev.* **2004**, *7*, 513.
8. (a) Skiles, J. W.; Gonnella, N. C.; Jeng, A. Y. *Curr. Med. Chem.* **2004**, *11*, 2911; (b) Rao, B. G. *Curr. Pharm. Des.* **2005**, *11*, 295; (c) Engel, C. K.; Pirard, B.; Schimanski, S.; Kirsch, R.; Habermann, J.; Klingler, O.; Schlotte, V.; Weithmann, K. U.; Wendt, K. U. *Chem. Biol.* **2005**, *12*, 181; (d) Pirard, B. *Drug Discovery Today* **2007**, *12*, 640.
9. High-throughput SPR imaging by Graffinity against the company's fragment/leadlike 110,000 compound library (www.graffinity.com).
10. Key interactions of **1** and **2**: π-Stacking with His222; 3 hydrogen bonds: Carbonyl oxygen of furanyl amide with the backbone amide of Leu185, methyl amide carbonyl oxygen with the backbone amide nitrogen of Tyr244 of the specificity loop, and the methyl amide with the backbone carbonyl of Gly183. Additional interaction for **2**: hydrogen bond between the carbonyl oxygen of the benzofuran carboxylate and the backbone amide nitrogen of Thr245. Thr245 is at the beginning of the specificity loop and conserved for some MMPs. The observed HB interaction may effect the conformation of the selectivity loop and therefore influence overall selectivity. However, since it is a backbone HB we considered the lipophilic interaction of the benzofuran within the S1′ pocket to be more important.Coordinates for co-structures deposited as 3I7G (compound **1**) and 3I7I (compound **2**) with the RCSB protein data bank.
11. Biological activity of the compounds against the catalytic domain of human MMP-1, -2, -3, -7, -8, -9, -10, -12, -13, and -14 (all MMPs purchased from BioMol except for MMP-13 which was made in house and refolded from E-coli) were assessed by using the EnzoLyte™ 520 Generic MMP Assay Kit (AnaSpec Inc.). This kit uses a 5-FAM/QXL™520 fluorescence resonance 10 energy transfer (FRET) peptide as an MMP substrate. In the intact FRET peptide, the fluorescence of 5-FAM is quenched by QXL™520. Upon cleavage into two separate fragments by MMPs, the fluorescence of 5-FAM is recovered, and can be monitored at excitation/emission wavelengths = 490 nm/520 nm. The assays are performed in a 96-well or 384-well microplate format. Reported IC_{50} values reflect an *n* of 2–5.